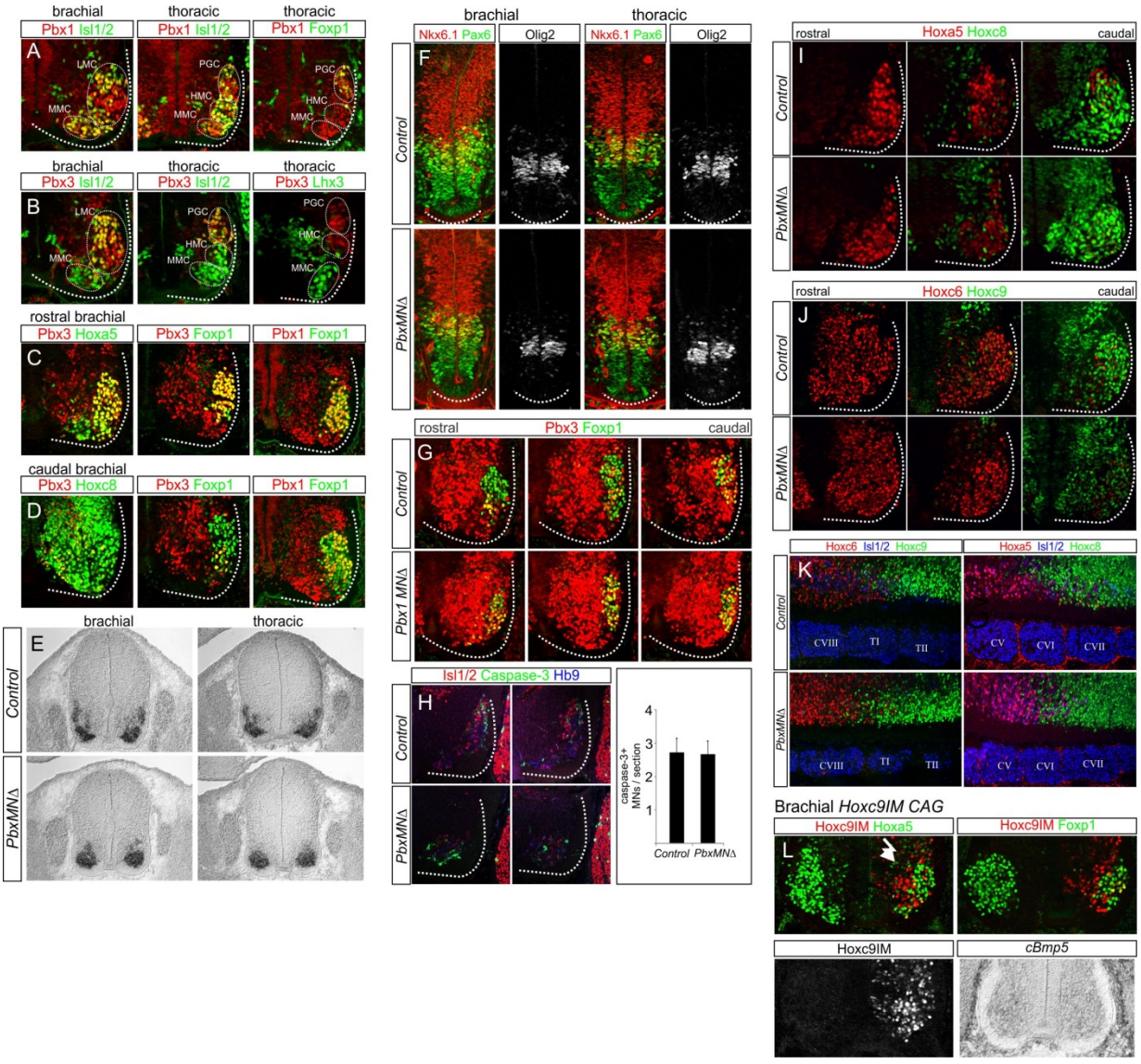

Figure S1, related to Figure 1. Pbx Expression Profiles in MNs and Effects of *Pbx* Mutations.
(A) Expression of Pbx1 in brachial and thoracic MNs at e11.5. Pbx1 is expressed in Isl1/2^{+} MNs, and Foxp1^{+} PGC neurons. (B) Expression of Pbx3 in brachial and thoracic MNs at e11.5. Pbx3 is expressed in Isl1/2^{+} MNs and Foxp1^{+} LMC neurons but is excluded from Foxp1^{-} MMC neurons. At thoracic levels Pbx3 is expressed in HMC and PGC neurons. (C) Rostral Hoxa5^{+} brachial LMC neurons express Pbx3 and Pbx1. (D) Caudal Hoxc8^{+} brachial LMC neurons express Pbx1 and Pbx3 in a subset of neurons. (E) Expression of *Vacht* in control and *Pbx* mutants at brachial and thoracic levels at e12.5. (F) Expression of MN progenitor markers in control and *Pbx* mutants at brachial and thoracic levels. (G) Derepression of Pbx3 in *Pbx1* mutants. Images show serial sections along the rostrocaudal axis. Pbx3 is normally absent or low in caudal brachial Hoxc8^{+} LMC neurons and excluded from MMC neurons. In *Pbx1*$^{MN\Delta}$ mice expression of Pbx3 is upregulated in both Foxp1^{+} MNs and MMC neurons. (H) Caspase3 staining at e12.5 in control and *Pbx* mutants. Graph on right shows average number of apoptotic MNs per section on one side of the spinal cord +/- SEM. (I-J) Serial sections showing boundaries between Hoxa5 and Hoxc8, and Hoxc6 and Hoxc9 are preserved in *Pbx* mutants. (K) Longitudinal sections showing Hox boundaries in control and *Pbx* mutants. Segmental level is determined by Isl1 staining of DRG. Segmental profiles appear to be preserved, although small changes in MN Hox boundaries may be present. (L) Effects of brachial misexpression of Hoxc9 IM. Hoxc9 IM represses Foxp1 and Hoxa5 but fails to generate ectopic *Bmp5*$^{+}$ PGC neurons.

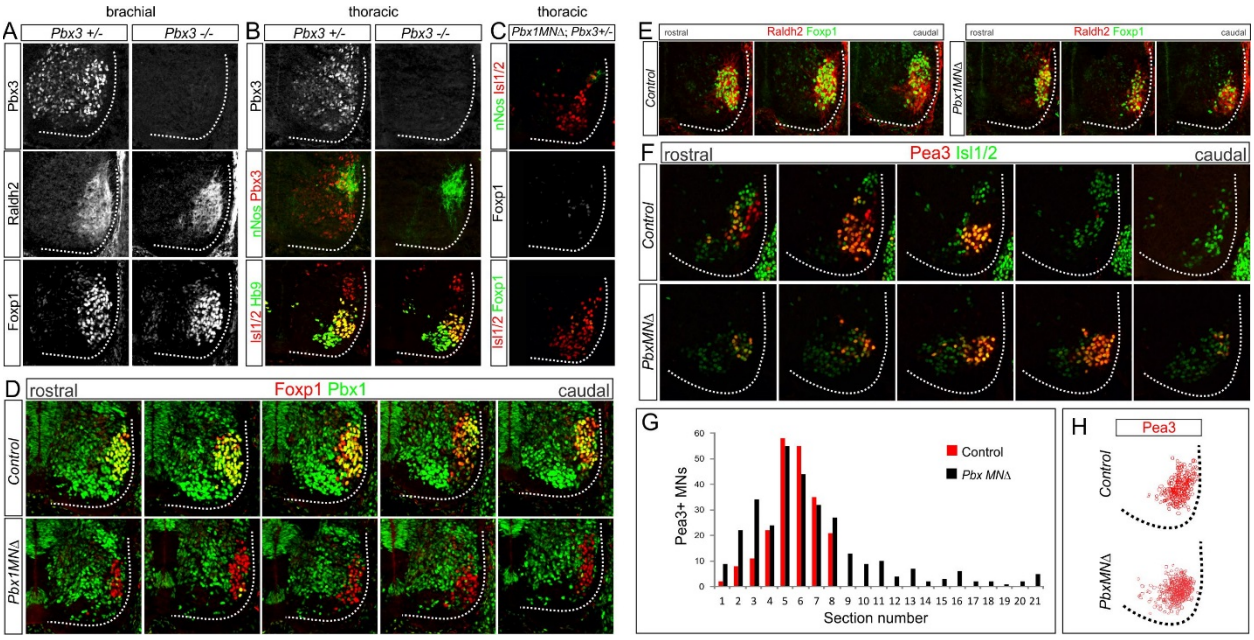

Figure S2, related to Figure 2. Effects of *Pbx* Mutation on MN Subtype Differentiation.
(A) LMC differentiation is preserved in *Pbx3-/-* mice at e12.5 as assessed by Raldh2 and Foxp1 expression. (B) At thoracic levels *Pbx3* mutants have a normal PGC as assessed by nNos expression. The differentiation of HMC neurons is also unaffected as assessed by Isl1/2, Hb9 co-expression. (C) Dose dependent loss of PGC neurons in $Pbx1^{MN\Delta}$, $Pbx3^{+/-}$ mutants, assessed by reduced nNos and Foxp1 expression. (D) In $Pbx1^{MN\Delta}$ mutants there is a reduction in the size of the LMC as assessed by Foxp1 expression. Images show sections along the rostrocaudal axis. (E) Reduction in $Foxp1^{+}$ $Raldh2^{+}$ LMC neurons in $Pbx1^{MN\Delta}$ mutants. (F) Expression of Pea3 in control and $Pbx^{MN\Delta}$ mutants. In $Pbx^{MN\Delta}$ mutants the Pea3 pool is present and extends to thoracic levels of the spinal cord. (G) Quantification of $Pea3^{+}$ MNs in control and $Pbx1^{MN\Delta}$ mutants along the rostrocaudal axis. (H) Pea3 neurons appear to be clustered in $Pbx1^{MN\Delta}$ mutants, likely due to the preservation of motor-pool specific clustering programs.

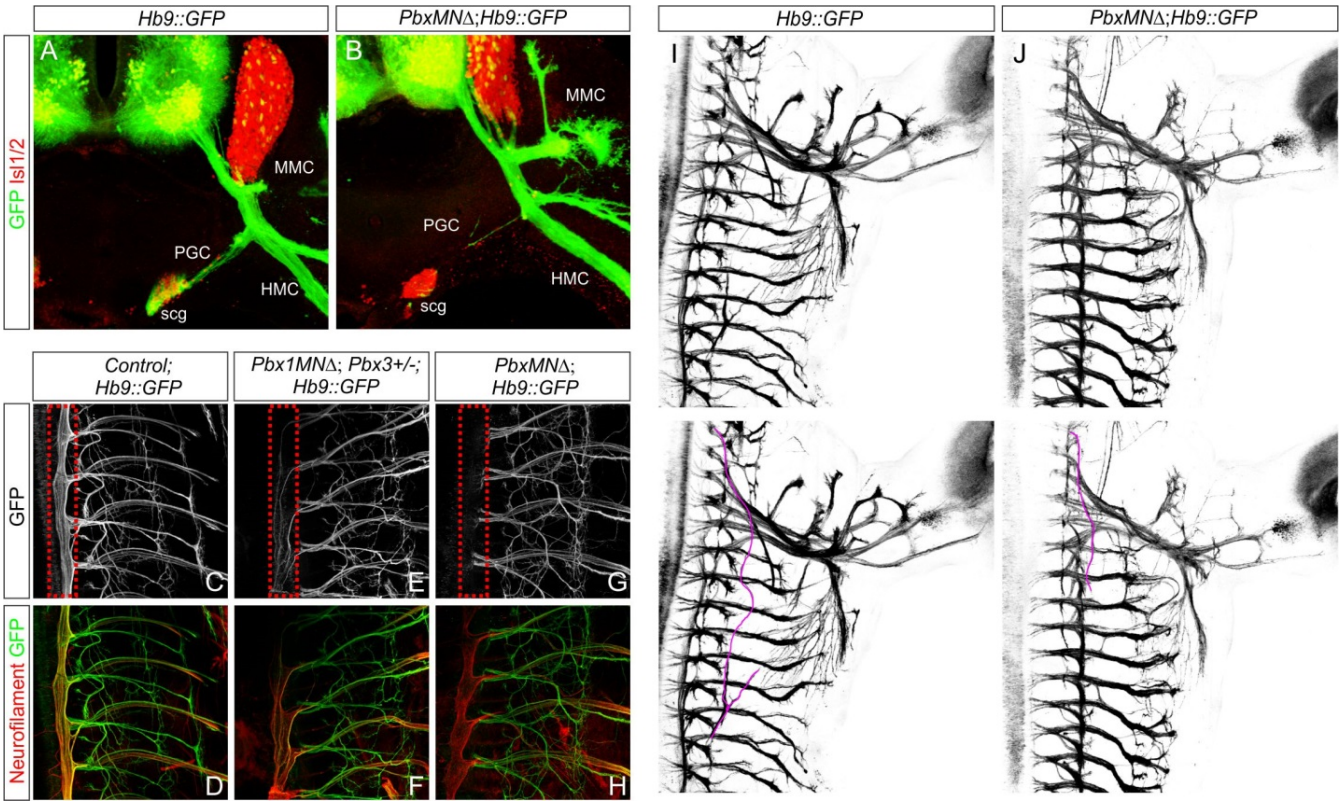

Figure S3, related to Figure3. Motor Axon Projections at Thoracic Levels in *Pbx*$^{MN\Delta}$ Mutants.
(A,B) Vibratome cross sections at thoracic levels showing projections of motor axons in control and *Pbx* mutants. Axons are GFP-labeled through breeding with *Hb9::GFP* mice. Projections originating from MMC, HMC and PGC neurons are indicated. PGC neurons target sympathetic chain ganglia (scg), and scg neurons are labeled with Isl1/2. In *Pbx* mutants, projections to scg are reduced. (C-H) Innervation pattern at thoracic levels in control and indicated *Pbx* mutants at e14.5. Projections originating from PGC neurons are markedly reduced in *Pbx1*$^{MN\Delta}$;*Pbx3*+/- and *Pbx*$^{MN\Delta}$ mice (indicated in red box). Neurofilament staining shows overall peripheral innervation pattern. (I,J) Ventral view of motor axon projections in control and *Pbx* mutants at e12.5. Bottom panels highlight the phrenic nerve in magenta, which is truncated in *Pbx* mutants.

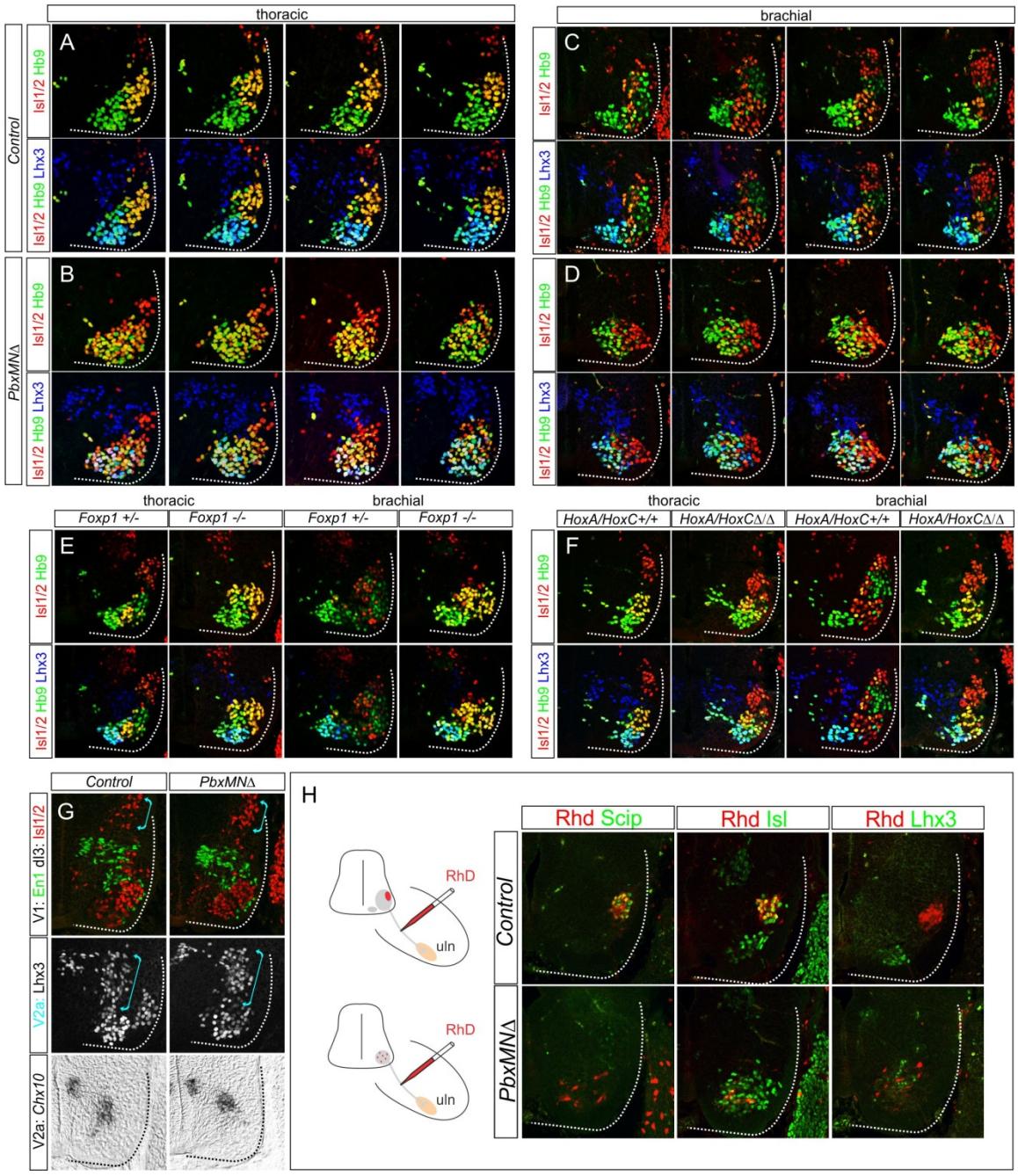

Figure S4, related to Figure 4. Columnar Disorganization in *Pbx* Mutants.
(A-D) MN columnar organization at brachial and thoracic levels in control and $Pbx^{MN\Delta}$ mice at e12.5. Images show Isl1/2;Hb9 coexpression (HMC) and Isl1/2;Hb9;Lhx3 staining of the sections shown in Figure 4A-H. (E) Analysis of *Foxp1* mutants at brachial and thoracic levels. Images show staining of indicated markers in the same sections shown in Figure 4L (F) Analysis of *HoxA/C* cluster mutants at brachial and thoracic levels. Images show staining of indicated markers in the same sections shown in Figure 4M. *HoxA/C* cluster mutants also contain a population of $Isl1/2^{+}$, $Foxp1^{-}$, $Lhx3^{-}$ MNs that are clustered. (G) Ventral interneuron identity and organization is preserved in *Pbx* mutants. Expression of En1 (a marker for V1 neurons), dorsal $Isl1^{+}$ neurons (dI3), dorsal $Lhx3^{+}$ neurons (V2a), and *Chx10* (V2a) is preserved in *Pbx* mutants. (H) Retrograde labeling from the ulnar nerve in control and *Pbx* mutants. In control mice ulnar MNs are $Scip^{+}$. In *Pbx* mutants, $Scip^{+}$ MNs are absent and brachial HMC-like neurons ($Isl1^{+}$, $Lhx3^{-}$) target the ulnar nerve and are dispersed within the spinal cord, similar to *Foxp1* mutants.

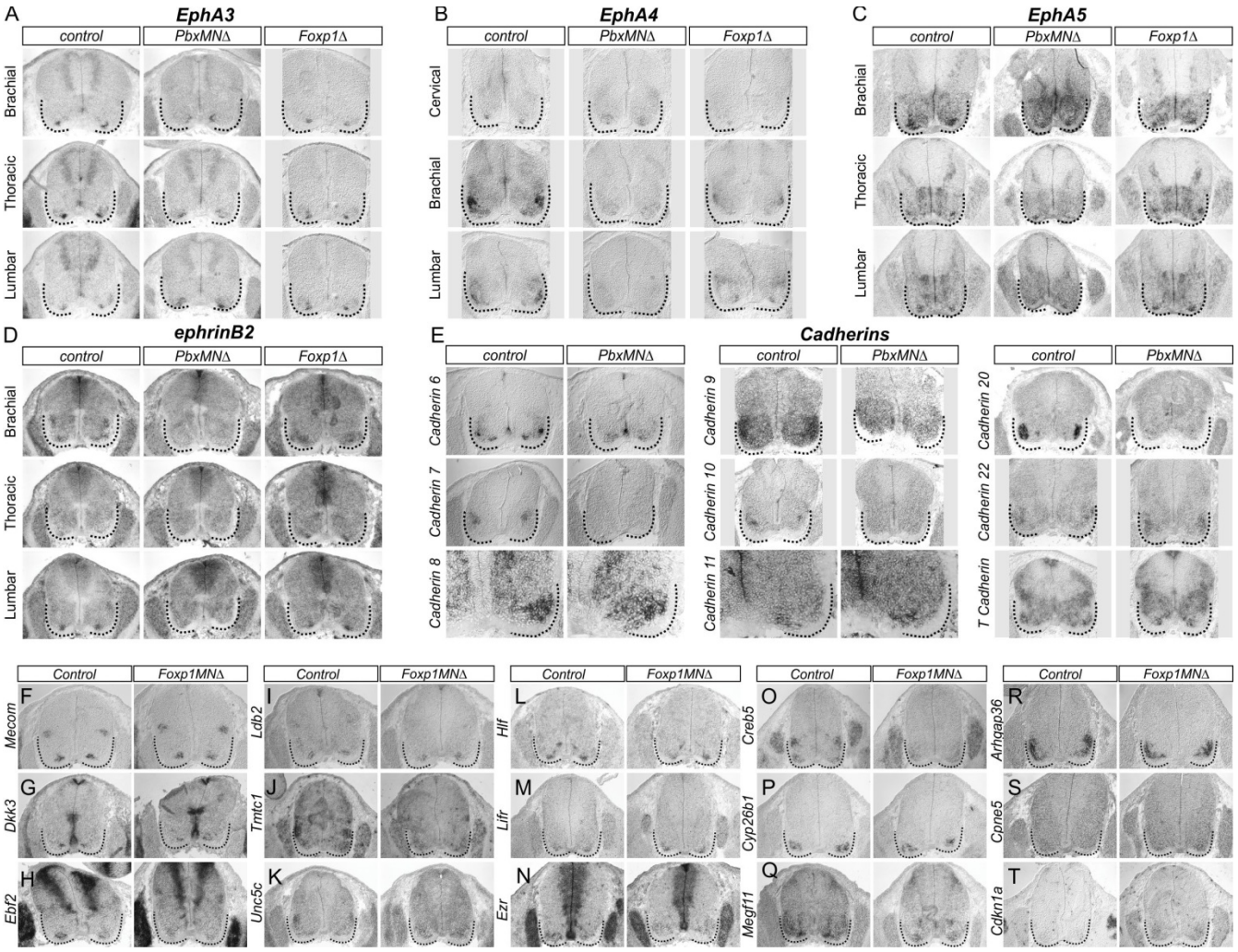

Figure S5, related to Figure 5. Analysis of Candidate Genes in *Pbx* and *Foxp1* Mutants.
(A-E) *In situ* hybridization analysis of *Eph/ephrin* and *cadherin* gene expression in *Pbx* and *Foxp1* mutants. All sections are e12.5 brachial spinal cord. (A,C) Expression of *EphA3* and *EphA5* was maintained in ventromedial neurons in *Pbx* and *Foxp1* mutants. (B) Expression of *Epha4* was lost in LMC neuron of *Foxp1* and *Pbx* mutants. (D) Expression of *ephrinB2* appears diminished in MMC neurons in *Pbx* mutants, but maintained in *Foxp1* mutants. (E) Expression of *cadherins* in *Pbx* mutants. LMC pool-specific *cadherin* expression is diminished in *Pbx* mutants, including loss of *Cadherin 6*, *Cadherin 7*, *Cadherin 9*, *Cadherin 10*, and *Cadherin 20* expression. Expression of *Cadherin 11* and *T Cadherin* does not appear to be diminished in ventromedial neurons in *Pbx* mutants. *Cadherin 8* expression by Pea3^{+} neurons is also preserved in *Pbx* mutants. (F-T) Analysis of selected Pbx target genes in *Foxp1* mutants. All sections are brachial spinal cord, except O and P, which are thoracic. Expression of *Mecom*, *Dkk3*, *Ebf2*, *Ldb2*, *Hlf*, *Lifr*, and *Cyp26b1* are maintained by MMC neurons. *Cpne5* and *Cdkn1a* are not upregulated.

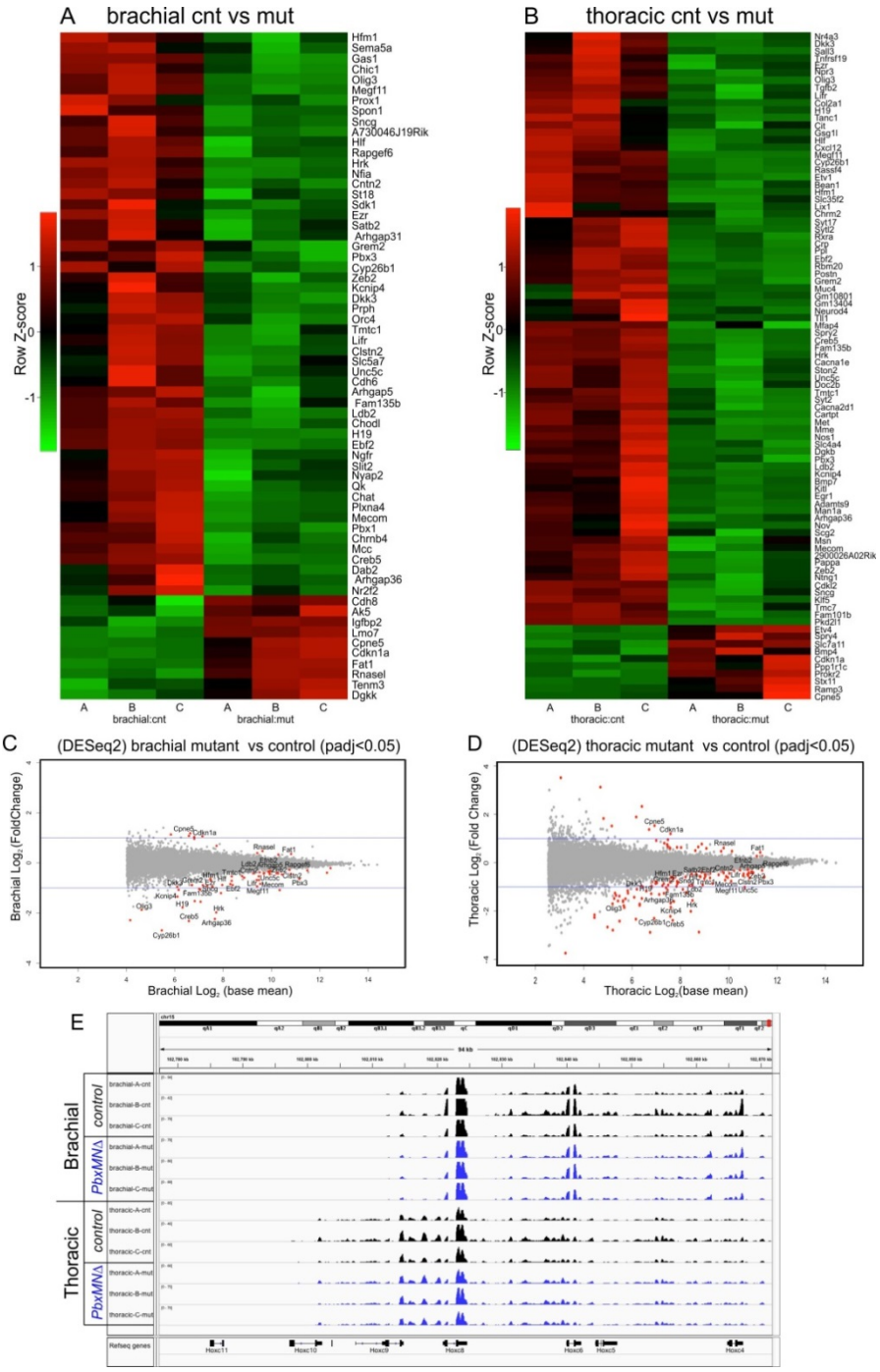

Figure S6, related to Figure 6. Analysis of Pbx Targets by RNAseq.
(A,B) Heat maps showing genes differentially expressed between control and *Pbx* mutants at brachial and thoracic levels with a padj<0.05 cutoff. (A) Brachial heatmap of 64 genes (padj <0.05, no FC cutoff) with 54 downregulated genes and 10 upregulated genes (B) Thoracic heatmap of 90 genes (padj <0.05, Log2FC >1 and < -0.5), 80 downregulated genes, not including *Cntn2*, *Clstn2*, *Rapgef6*, *Arhgap5* (log2 fold change < -0.3) and 10 upregulated genes, not showing *Fat1* and *RnaseL* (log2 fold change >0.3). (C,D) MA plots with padj<0.05 genes in red with 31 shared genes between brachial and thoracic labeled shown in red and all other genes in gray.(E) Read counts (CPM) for genes within the *HoxC* locus in control and *Pbx* mutants at brachial and thoracic levels. Reads for each of the three pools used for RNAseq are shown.

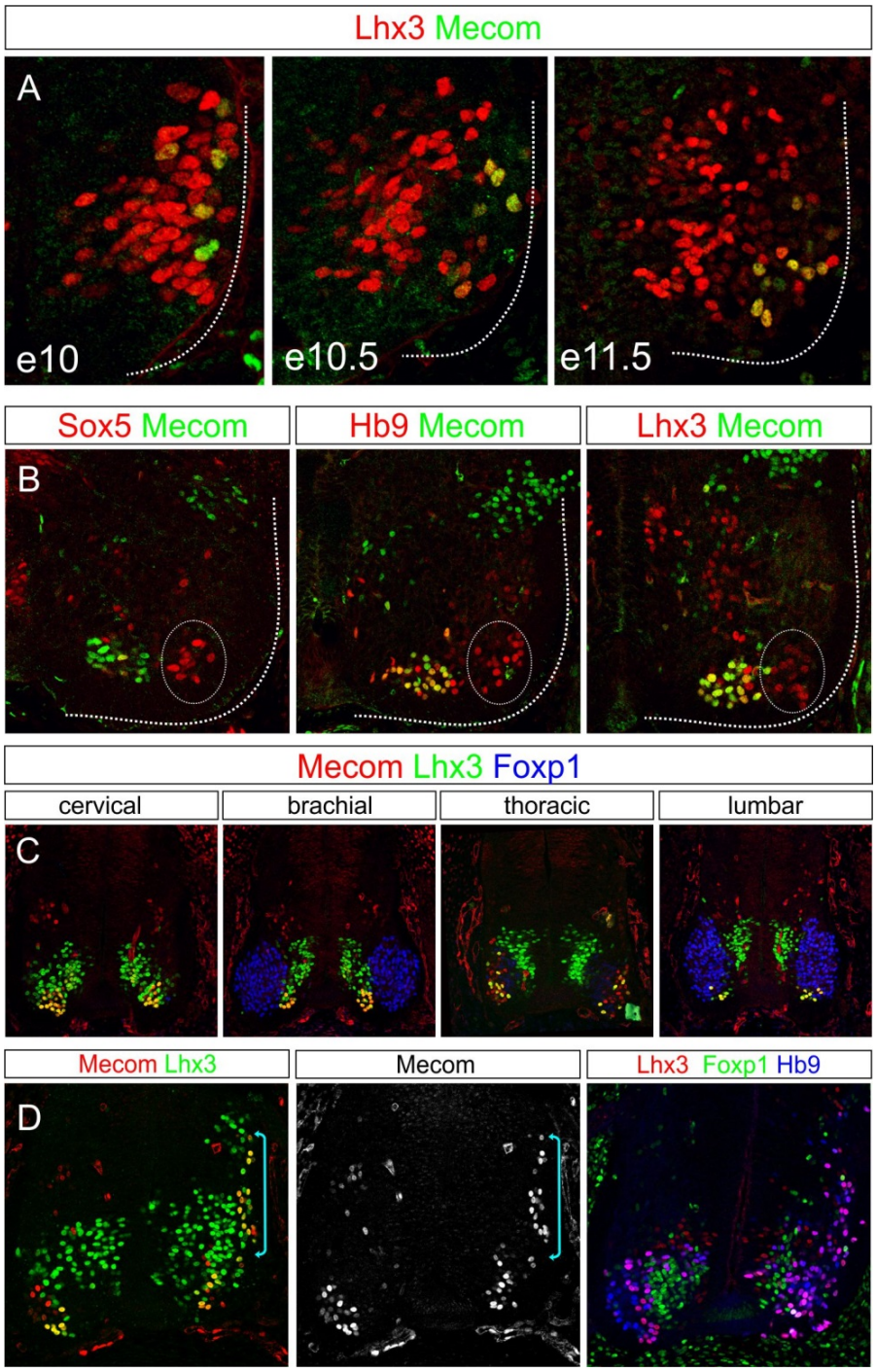

Figure S7, related to Figure 7. Expression of Mecom in MNs.
(A) Ontogeny of Mecom expression between e10-e11.5. Mecom is expressed in mature Lhx3^{+} MNs but not detected in Lhx3^{+} MN precursors or V2 interneurons. (B) Mecom is excluded from non-MMC Lhx3^{+} populations located at rostral cervical levels, including the Sox5^{+} pool (outlined). (C) Expression of Mecom in Lhx3^{+} MMC neurons in chick at cervical, brachial, thoracic and lumbar levels at st28. (D) Coelectroporation of Lhx3 and Hb9 induces Mecom expression in the dorsal spinal cord as indicated by cyan brackets.

Table S1, related to Figure 5. RNA seq data showing control brachial versus control thoracic genes padj<0.05, fold change >1 or <-1.

Table S2, related to Figure 5. RNA seq data showing control thoracic versus *Pbx* mutant thoracic genes padj<0.05.

Table S3, related to Figure 5. RNA seq data showing control brachial versus *Pbx* mutant brachial genes padj<0.05.

Supplemental Experimental Procedures

Antibodies

Additional antibodies were obtained as follows: rabbit anti-nNos (Immunostar, RRID: AB_572255), rabbit anti-Evi1/Mecom (Cell Signaling, RRID: AB_2184098), goat anti-Scip (Santa Cruz, RRID: AB_2268536), rabbit anti-Pea3 (Silvia Arber, FMI), rabbit anti-Pbx1 (Cell Signaling, RRID: AB_2160295 and Santa Cruz, sc-8707-R), rabbit anti-Pbx2 (Santa Cruz, RRID: AB_2283521), chicken and rabbit anti-GFP (Invitrogen, RRID: AB_2534023 and RRID: AB_221570), rabbit anti-NF (SYSY, RRID: AB_887743), rabbit anti-synaptophysin (Invitrogen), Alexa 594–conjugated bungarotoxin (Invitrogen, RRID: AB_2313931), goat anti-HRP (Jackson Immunoresearch, RRID: AB_2314648), mouse anti-HA (Covance, RRID: AB_2616042), and Caspase 3 (Cell Signaling, RRID: AB_331439).

Analysis of Motor Neuron Columnar Intermixing

Intermixing of MMC and HMC neurons was calculated as described previously (Demireva et al., 2011). Motor neurons expressing markers of MMC and HMC identity were identified by transcription factor expression in 12 μm sections of e12.5 spinal cord. The incidence of MMC→HMC and HMC→MMC transgression was determined by constructing a perimeter trace that incorporates each of the nuclei of neurons of one motor column, and then scoring the number of neurons from the other column that invade this perimeter, expressed as a fraction of the total number of potential invaders. From these values we obtained a columnar mixing index (Cmi) which represents the incidence of transgression as a fraction of maximal possible degree of columnar intermixing (Cmax). The value for Cmax was calculated from simulated random distribution plots of the two columnar subtypes, obtained using experimentally derived MMC and HMC neuronal numbers and packing densities.

Retrograde Labeling

Retrograde labeling of motor neurons was performed as described (Dasen et al., 2003). 3000 MW lysine-fixable dextran-tetramethylrhodamine (RhD, Molecular Probes) or horseradish peroxidase (HRP, Roche) was injected into severed nerves or muscles of e12.5 embryos. Prior to injections, embryos were decapitated, eviscerated, and dissected to remove the epidermis dorsal to the spinal cord. To aid in the identification of nerves, we used GFP fluorescence from *Hb9::GFP* transgenic mouse embryos, visualized using a MVX10 wide-field fluorescent macroscope (Olympus). Embryos were incubated for 3–5 hr in oxygenated F12/DMEM (50:50) solution at 32–34°C and subsequently fixed in 4% paraformaldehyde.

Dissections and Cell Dissociation and FACS

Motor neurons were isolated from e12.5 *PbxMNΔ; Hb9::GFP* and control *Hb9::GFP* mice at brachial and thoracic levels. Brachial MNs were isolated from segments C2-T1, thoracic MNs from T2-T11. Neurons were dissociated using papain and filtered for sorting. A GFP negative spinal cord was also included as a negative control for the FACs setup. To restrict sorting to MNs and not interneurons with low *Hb9::GFP* expression, a control *Hb9::GFP* spinal cord in which MNs were removed by dissection was also used. This sample provided a threshold cutoff to restrict low GFP expressing cells from being purified. Cells were collected into Arcturus Picopure extraction buffer, and immediately processed for RNA isolation.

RNA Extraction, Library Preparation and RNA Sequencing

RNA was extracted from purified MNs, using the Arcturus Picopure RNA isolation kit, 3 RNA samples of each genotype were pooled, and used to prepare 12 bar coded libraries. Prior to pooling RNA quality and quantity were measured with an Agilent Picochip using a Bioanalyzer, all samples had high quality scores between 9-10 RIN. For library preparation 10ng of pooled total RNA was used, and cDNA was amplified using Nugene's Ovation RNA-Seq System V2 kit (Part N0. 7102), 100 ng of cDNA were used as input to prepare the libraries, using the Ovation Ultralow Library system (Nugen, Parts No 0303-05 and 0330-31), and amplified by 10 cycles of PCR. We then performed RNAseq analysis to identify candidate genes. The samples were mixed into two pools and run in two 50-nucleotide paired-end read rapid run flow cell lanes with the Illumina HiSeq 2500 sequencer, to generate on average 74 and 101 million reads passing filter for forelimb and thoracic samples, respectively. This analysis yielded 64 brachial and 124 thoracic genes that were differentially expressed (padj. < 0.05) between control and *PbxMNΔ* mice. With a less stringent cut off of a (P-value < 0.05) this analysis yielded 687 brachial and 834 thoracic genes that were differentially expressed between control and *PbxMNΔ* mice.